28 GHz Indoor Channel Measurements and Modelling in Laboratory Environment Using Directional Antennas

(Invited Paper)

Xianyue Wu[1,3], Yan Zhang[1,2], Cheng-Xiang Wang[1,3], George Goussetis[1],
el-Hadi M. Aggoune[3] and Mohammed M. Alwakeel[3]

[1] School of Engineering & Physical Sciences, Heriot-Watt University Edinburgh EH14 4AS, UK
[2] School of Information and Electronics, Beijing Institute of Technology, Beijing 100081, China
[3] Sensor Networks and Cellular Systems Research Center, University of Tabuk, 71491 Tabuk, Saudi Arabia
Email: [1]x.wu@hw.ac.uk, y.zhang@hw.ac.uk, cheng-xiang.wang@hw.ac.uk, g.goussetis@hw.ac.uk,
[2]haggoune.sncs@ut.edu.sa, alwakeel@ut.edu.sa

Abstract—The millimeter-wave band will be one of the key components for the fifth generation (5G) wireless communication systems. A radio channel measurement was conducted at 28 GHz in a laboratory environment. Two horn antennas were used with a vector network analyzer. The transmitter antenna was fixed in one direction while the receiver antenna was rotated 360° in azimuth in the measurement. The space-alternating generalized expectation-maximization algorithm was utilized for the rotated directional antenna scenario to estimate channel parameters of multipath components. Power delay profile, power angle profile and root mean square delay spread were obtained from the measured results. The Saleh-Valenzuela model was used to characterize the measured channel and the intra-cluster parameters were extracted.

Index Terms—millimeter-wave, 5G, channel measurement, channel modelling

I. INTRODUCTION

Wireless communication networks are faced with new shortcomings as Internet usages are proliferating. Future networks will have to support high capacity and massive connectivity with an increasingly diverse set of services, applications and users such as Machine-to-Machine (M2M) and Internet of things (IoT). Also, the flexible and efficient use of all spectrum and resources are required to accommodate widely different network deployment scenarios. These requirements envisioned for what are now being called fifth-generation (5G) wireless communication systems. To address these challenges, there has been growing interest in moving up frequency into millimeter wave (mmWave) where enormous bandwidths are available. The mmWave approach can achieve much higher data rates by using simple air interfaces due to large bandwidth. In addition, by virtue of the vast available and unexploited bandwidth, mmWave systems can easily satisfy higher system capacity requirement.

Recently, there has been extensive research on mmWave outdoor cellular communications. In [1]–[3], the measurements were conducted at 28, 38 and 73 GHz in the urban environments. Results show by using directional or adaptive-beam antennas, mmWave signals are potentially viable at distances of 100-200 meters, even in none-line-of-sight (NLOS) scenarios. Besides, the mmWave systems can provide at least an order of magnitude in capacity over current state-of-the-art LTE systems, at least for outdoor coverage.

The current cellular communication systems normally use an outdoor base station (BS) in the middle of a cell to communicate with mobile users, no matter whether they stay indoors or outdoors. For indoor users communicating with the outdoor BS, the signals have to go through building walls, and this causes very high penetration loss, which significantly degrades the data rate, spectral efficiency, and energy efficiency of wireless transmissions. At mmWave frequencies, this situation will be even worse due to high penetration loss through building walls. Therefore, outdoor and indoor scenarios will be probably separated in 5G cellular architecture [4].

Most of the research on indoor mmWave channel measurements and modelling in the literature were carried out at 60 GHz. This is mainly because there are several GHz spectrum around 60 GHz was freed for unlicensed use by spectrum regulators and high oxygen attenuation prevents it for outdoor usage. Two IEEE standards have been proposed for 60 GHz indoor wireless communications, namely, IEEE 802.11ad and IEEE 802.15.3c. The indoor channel characterization at this frequency band has been well studied. However, there is very limited studies for mmWave indoor channel below 60 GHz. This work conducted indoor channel measurements at 28 GHz. The motivation of selecting this frequency is to study feasibility of reusing 28 GHz for indoor applications while this frequency was proposed for outdoor cellular communications recently. The cost efficiency is a major concern for 5G systems, which can be significant improved by reusing of either spectrum or hardware.

For mmWave wireless communications, directional antennas are implemented to overcome fading margins in the link budget. Beam-steering or beam-forming techniques are

proposed to solve inherent coverage problems associated with these narrow beam antennas [5]. Samsung has announced its 60 GHz WiFi technology based on wide-coverage beam-forming antennas with mirco beam-forming technology recently [6]. Therefore, we adopted beam-steering approach with the high gain antenna in the channel measurement to simulate real scenarios.

In the channel modelling, there are generally two types of method to resolve the multipath components in space. One is using the linear (virtual) array with omni-directional elements. The angle of departure (AoD) and angle of arrival (AoA) estimates for the multipath components were obtained using high resolution signal processing methods such as the space-alternating generalized expectation-maximization (SAGE) algorithm [7]. The other method is based on steering the highly directional antenna in the measurement. The half power beamwidth of this kind of antenna is very narrow, so it can resolve multipath components in space directly [8]. In the proposed work, in order to improve dynamic range of the measurement system, the combination of two methods were adopted. A circular virtual array of a rotational directional antenna was used in the channel measurement and the SAGE algorithm was utilized for channel parameter estimation.

The paper is organized as follows. Section II presents the experimental setup for channel measurement. The measured results and the analysis are presented in Section III. Section IV relates the channel modelling and Section V summarizes this work.

II. Indoor Channel Measurement

The indoor measurement was conducted in a laboratory environment as shown in Fig. 1. The size of the room is about $7 \times 10 \times 3.5$ m^3. The lab is furnished with multiple chairs, desks and a table. In addition, the room is equipped with several computers and electronic devices. The walls are typical plasterboard walls, and the floor and ceiling are made of concrete. Two standard horn antennas are used for transmitter and receiver, respectively. The radiation pattern of the horn antenna is shown in Fig. 2. The gain of the antenna is 18.52 dBi at 28 GHz. The 3-dB beamwidth of the horn antenna is about $20°$ at both E and H planes. The Tx antenna was at a fixed position. The Rx antenna was placed on a tripod and rotated clockwise from $0°$ to $360°$ in azimuth with the step of $15°$. The heights of Tx and Rx antennas were both at 1.1 m. The lab layout and antenna positions are shown in Fig. 3. Although there was a table in between the transmitter and receiver, the height of table was below the height of antennas. So, the Rx and Tx were in the line-of-sight (LOS) condition with 4 m separation. During the measurement, the environment was kept static. Two 5-m long coaxial cables were used to connect Tx and Rx antennas to an Agilent N5245A vector network analyzer (VNA). The measured frequency range is 27.5 GHz to 28.5 GHz using 3201 frequency points. The time resolution of this setup is 1 ns. The output power of VNA was 15 dBm and intermediate frequency (IF) filter bandwith was

1 kHz. The duration of each sweep was 2.95 s.
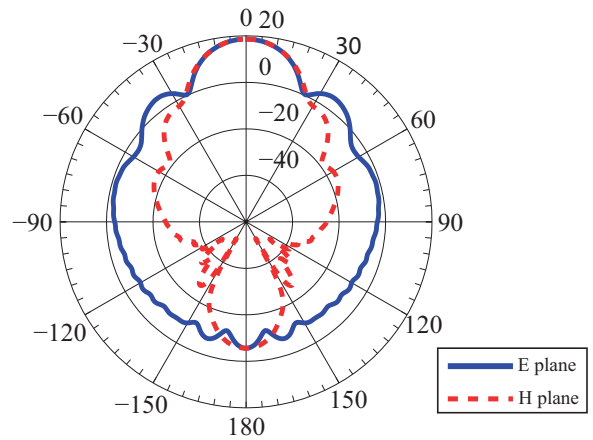

Fig. 1. Lab environment and measurement setup.

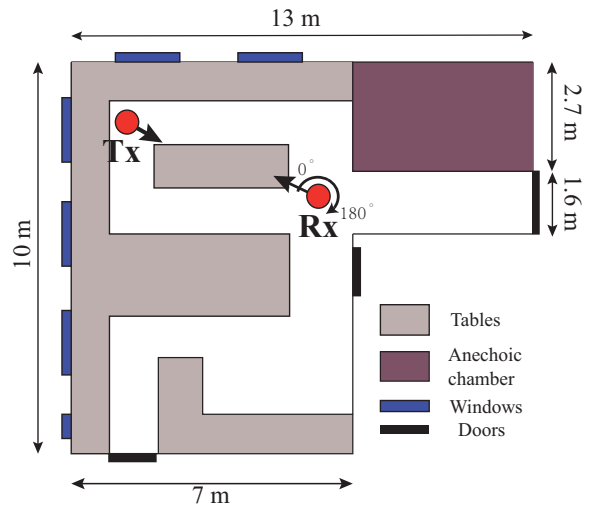Fig. 2. Radiation pattern of horn antenna at 28 GHz.

Fig. 3. Lab environment layout.

III. Measurement Results

A. Power Delay Profile

The power delay profile (PDP) was computed as the inverse Fourier transform of the measured channel transfer functions. The hanning window was applied to the measured data before the transform to suppress the undesired side lobes and improve the dynamic range in the time domain. Fig. 4 shows the 3D plot of power delay profile, where θ is Rx antenna rotational angle. As shown in the figure, the peak power is received at $0°$ for the LOS path and second peak is observed at $\pm180°$, which are reflections of LOS path. And there are some other minor multipaths can be observed.
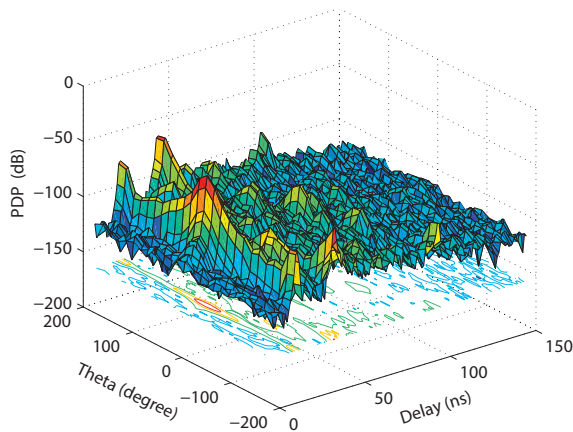

Fig. 4. Power delay profile plot in 3D.

B. Synthesized Power Delay Profile

A method was proposed for synthesizing the directional PDP to a omni-directional-like one [9]. This method allows each directional measurement to be aligned in time domain and composed PDPs covering all $360°$ directions can be obtained. If at a specific time delay, multiple directional PDPs are overlapped, only the multipath component (MPC) with maximum peak power is selected because the dominant MPC on dedicated angle should be considered for synthesized PDPs. The method is illustrated in Fig. 5.

C. Root Mean Square (RMS) Delay Spread

The RMS delay spread (second-order moment) can also be computed from the composed PDP by

$$\tau_{rms} = \sqrt{\frac{\sum\limits_{n} \mathrm{PDP}(\tau_n)\tau_n^2}{\sum\limits_{n} \mathrm{PDP}(\tau_n)} - \left(\frac{\sum\limits_{n} \mathrm{PDP}(\tau_n)\tau_n}{\sum\limits_{n} \mathrm{PDP}(\tau_n)}\right)^2} \quad (1)$$

where $\mathrm{PDP}(\tau_n)$ are the components of the PDP within a threshold and τ_n are their corresponding delay. A threshold of 60 dB below the peak was selected to compute RMS delay spread. The calculated RMS delay spread from synthesized PDP is 4.50 ns. This value is relatively small because the fixed direction of the transmitting antenna.
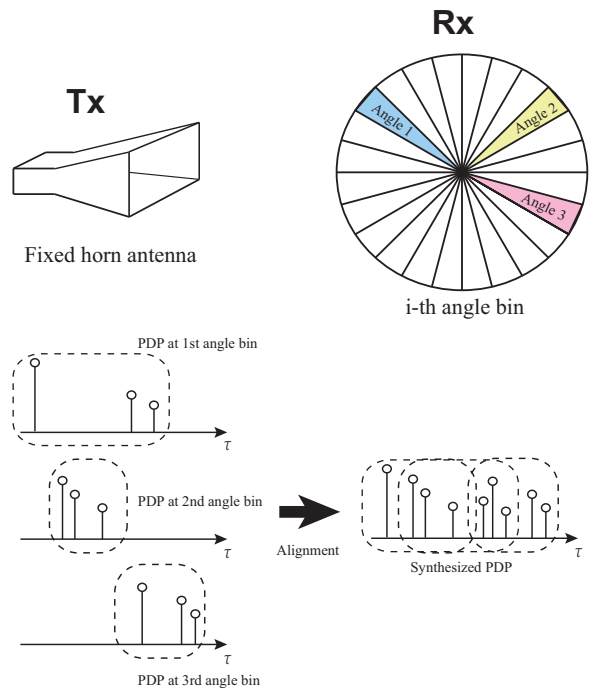

Fig. 5. (a) Measurements in each angle bin at receiver and fixed angle at transmitter. (b) The directional PDP are synchronized and superimposed. The synthesized delay profile is shown as the output.

D. SAGE Algorithm

In order to estimate the AoAs, the SAGE algorithm was applied on the previously computed PDP data. Unlike previous studies which use the linear virtual array of omni-directional elements, we used the rotated directional antenna in the measurements. The antenna was considered as a virtual 24-element circular array. Each element points to a specific direction with high directivity. The spacings between elements were assumed to be zero. Based on this assumption, a modification was applied to the original SAGE algorithm [10], where the M-dimensional vector-valued function of the steering vector of the array is defined as

$$c(\phi) = [c_1(\phi),...,c_M(\phi)]^T \quad (2)$$

Its components are given by

$$c_m(\phi) = f_m(\phi)\exp\{j2\pi\lambda^{-1}\langle e(\phi), r_m \rangle\} \quad (3)$$

with λ, $e(\phi)$, $f_m(\phi)$ denoting the wavelength, the unit vector in IR^2 pointing toward the direction determined by ϕ, and the complex electric field pattern of the mth antenna element, respectively. In the proposed algorithm $c_m(\phi) = f_m(\phi)$ which is the antenna radiation pattern when the antenna points to a specific angle, i.e. the rotated radiation pattern of that shown in Fig. 2. The channel parameters of ith path components including complex amplitude, delay and angle of arrival in azimuth were estimated using the proposed SAGE algorithm. The number of estimated path is set to 200. Fig. 6 shows the estimated delay-azimuth spread function.
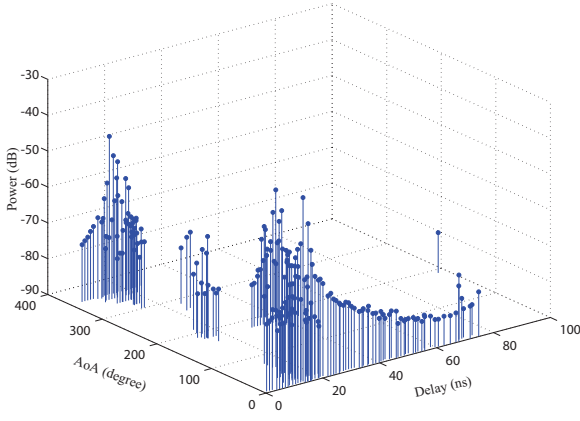
Fig. 6. Estimated delay-azimuth spread function using SAGE algorithm.

The power delay profile and power angle profile (PAP) were obtained using the estimated channel parameters. Fig. 7 shows the power delay profile using estimated results compared with synthesized results described in Section III-B. A good agreement can be observed, which validated the proposed SAGE algorithm.
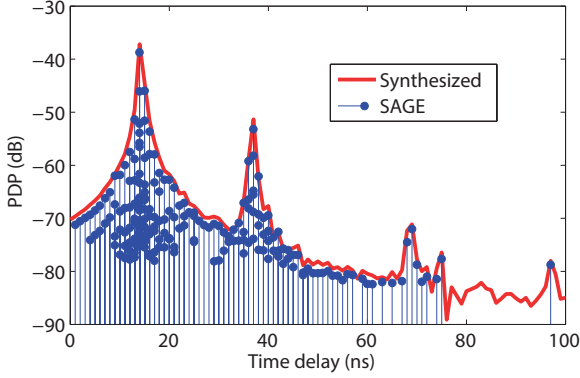

Fig. 7. PDP: synthesized measurement results vs. estimated using SAGE algorithm

Fig. 8 shows the estimated power angle profile using SAGE algorithm. Two angles with significant power can be observed. One is at $0°$ or $360°$, which is for the LOS path. The other is at $180°$, which is due to the reflection from the wall. Some minor multipaths can be observed in the angle ranges of $40° - 70°$ and $260° - 320°$. However, because of the fixed direction of the transmitting antenna, a relative small region of the room was covered by radio propagation and few number of multipaths were received.

IV. CHANNEL MODELLING

The Saleh-Valenzuela (S-V) channel model [11] is used to model the measured results. The channel impulse response for the S-V model may be written as:

$$h(t) = \sum_i A^{(i)} C^{(i)}(t - T^{(i)})$$
$$C^{(i)}(t) = \sum_k \alpha^{(i,k)} \delta(t - \tau^{(i,k)})$$
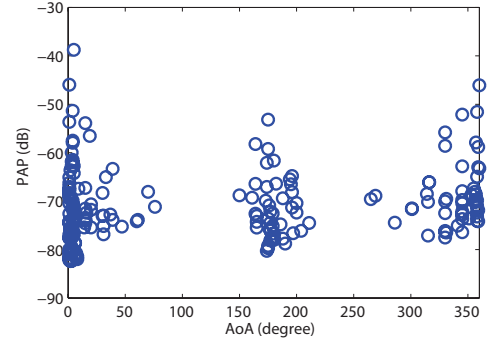
(4)

Fig. 8. Estimated power angle profile using SAGE algorithm

where:
- h is a generated channel impulse response.
- t is time at receiver.
- $A^{(i)}$ and $C^{(i)}$ are the gain and the channel impulse response for i-th cluster respectively.
- $\delta(\cdot)$ is the Dirac delta function.
- $T^{(i)}$ is time coordinate of i-th cluster.
- $\alpha^{(i,k)}$ is the amplitude of the k-th ray of i-th cluster.
- $\tau^{(i,k)}$ is relative time coordinate of k-th ray of i-th cluster.

Based on 60 GHz WLAN channel modelling in IEEE 802.11ad standard [12], the channel is characterized by inter-cluster and intra-cluster parameters. The intra-cluster time domain parameters can be modelled as shown in Fig. 9.
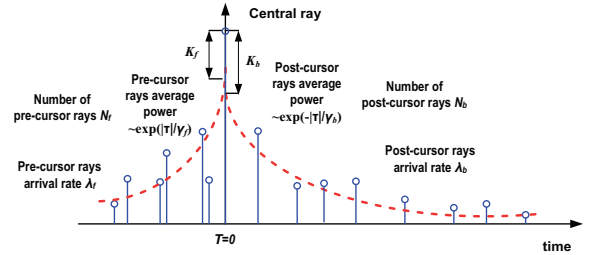

Fig. 9. Time domain model of the cluster [12].

The cluster consists of a central ray $\alpha^{(i,0)}$ with fixed amplitude and pre-cursor $\alpha^{(i,-N_f)}$ ... $\alpha^{(i,-1)}$ and post-cursor rays $\alpha^{(i,1)}$ ... $\alpha^{(i,N_b)}$. The central ray $\alpha^{(i,0)}$ was selected as the ray with highest amplitude in the cluster. The number of pre-cursor rays N_f and post-cursor rays N_b can be derived from measurements. Pre-cursor and post-cursor rays are modelled as two Poisson processes with arrival rates λ_f and λ_b, respectively. The average amplitudes A_f and A_b of the pre-cursor and post-cursor rays decay exponentially with power decay times γ_f and γ_b, respectively.

$$A_f(\tau) = A_f(0)e^{|\tau|/\gamma_f}$$
$$A_b(\tau) = A_b(0)e^{-|\tau|/\gamma_b}$$

(5)

The amplitudes of the pre-cursor and post-cursor rays are coupled with the amplitude of the central ray of the cluster

Parameter	Notation	Cluster 1	Cluster 2
Pre-cursor rays K-factor	K_f	12.8 dB	6.1 dB
Pre-cursor rays power decay time	γ_f	6.6 ns	12.8 ns
Pre-cursor arrival rate	λ_f	1ns^{-1}	1ns^{-1}
Number of pre-cursor rays	N_f	13	12
Post-cursor rays K-factor	K_b	7.4 dB	8.9 dB
Post-cursor rays power decay time	γ_b	3.6 ns	5.1 ns
Post-cursor arrival rate	λ_b	1ns^{-1}	1ns^{-1}
Number of post-cursor rays	N_b	11	11

$\alpha^{(i,0)}$ by Rician K-factors that are defined as:

$$
\begin{aligned}
K_f &= 20\log_{10}\left|\frac{\alpha^{(i,0)}}{A_f(0)}\right| \\
K_b &= 20\log_{10}\left|\frac{\alpha^{(i,0)}}{A_b(0)}\right|
\end{aligned}
\quad (6)
$$

In this study, the K-means algorithm [13] was utilized for clustering of estimated multipath components based on measurement results. As shown in Fig. 10, three clusters are identified in delay domain. If there are multiple MPCs arriving at a specific delay from different AoAs, the weighted vector sum was calculated based on the radiation patterns with corresponding angles.
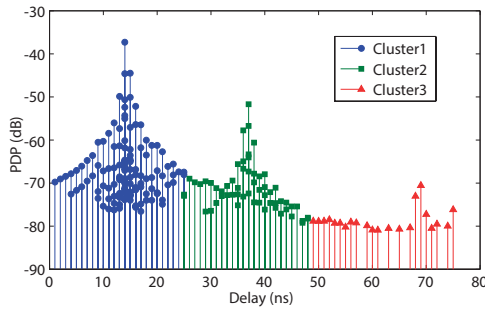

Fig. 10. Multipath component clustering in time domain.

Because Cluster 3 is too weak, only Cluster 1 and Cluster 2 were modelled. The intra-cluster parameters for Cluster 1 and Cluster 2 are summarized in Table I. Another important parameter of this model is cluster gains $A^{(i)}$, which can be calculated as [12]:

$$
A^{(i)} = \begin{cases} \lambda/(4\pi d) & \text{for LOS ray} \\ g^{(i)}\pi/(4\pi(d+R)); R = c\cdot t & \text{for NLOS clusters} \end{cases}
$$

where λ is a wavelength (10 mm), d is a distance between TX and RX (along LOS path), $g^{(i)}$ is a reflection loss, R is a total distance along the cluster path decreased by d, R is calculated as a product of time of arrival relatively LOS and the speed of light. In the proposed scenario, only $A^{(0)}$ and $A^{(1)}$ need to be calculated for the LOS ray and the first order reflection at angle of arrival of 180°, where d is 4 m, R is 6.9 m but $g^{(i)}$ need be further investigated. There results can be used for a reference for 28 GHz indoor wireless system design.

V. CONCLUSION

In this paper, a 28 GHz channel measurements were conducted in an indoor environment using two horn antennas. Based on authors' knowledge, this frequency is seldom explored for indoor wireless communications. The rotated horn antenna was considered as a virtual circular array. A modified SAGE algorithm was applied to estimate channel parameters for multipath components. The power delay profiles and the power angle profiles were obtained. A good agreement between the SAGE estimated PDP and the synthesized PDP can be observed which validated the proposed SAGE algorithm. The measured results were modelled using the Saleh-Valenzuela channel model in delay domain and the intra-cluster parameters were extracted. The more wider radiation angle for the transmitting antenna will be considered in the later study.

ACKNOWLEDGMENT

REFERENCES

[1] T. Rappaport, S. Sun, R. Mayzus, H. Zhao, Y. Azar, K. Wang, G. Wong, J. Schulz, M. Samimi, and F. Gutierrez, "Millimeter Wave Mobile Communications for 5G Cellular: It Will Work!" *IEEE Access*, vol. 1, pp. 335–349, 2013.

[2] T. Rappaport, F. Gutierrez, E. Ben-Dor, J. Murdock, Y. Qiao, and J. Tamir, "Broadband millimeter-wave propagation measurements and models using adaptive-beam antennas for outdoor urban cellular communications," *IEEE Transactions on Antennas and Propagation*, vol. 61, no. 4, pp. 1850–1859, April 2013.

[3] S. Rangan, T. Rappaport, and E. Erkip, "Millimeter-wave cellular wireless networks: Potentials and challenges," *Proceedings of the IEEE*, vol. 102, no. 3, pp. 366–385, March 2014.

[4] C.-X. Wang, F. Haider, X. Gao, X.-H. You, Y. Yang, D. Yuan, H. Aggoune, H. Haas, S. Fletcher, and E. Hepsaydir, "Cellular architecture and key technologies for 5G wireless communication networks," *IEEE Communications Magazine*, vol. 52, no. 2, pp. 122–130, February 2014.

[5] R. Daniels and R. Heath, "60 GHz wireless communications: emerging requirements and design recommendations," *IEEE Vehicular Technology Magazine*, vol. 2, no. 3, pp. 41–50, Sept 2007.

[6] "Samsung Electronics 60GHz Wi-Fi Technology Accelerates Data Transmission by Five Times," http://global.samsungtomorrow.com/?p=43234, 2014, [Online; accessed 13-October-2014].

[7] C. Gustafson, K. Haneda, S. Wyne, and F. Tufvesson, "On mm-wave multipath clustering and channel modeling," *IEEE Transactions on Antennas and Propagation*, vol. 62, no. 3, pp. 1445–1455, March 2014.

[8] H. Xu, V. Kukshya, and T. Rappaport, "Spatial and temporal characteristics of 60-GHz indoor channels," *IEEE Journal on Selected Areas in Communications*, vol. 20, no. 3, pp. 620–630, Apr 2002.

[9] S. Hur, Y.-J. Cho, J. Lee, N.-G. Kang, J. Park, and H. Benn, "Synchronous channel sounder using horn antenna and indoor measurements on 28 GHz," in *2014 IEEE International Black Sea Conference on Communications and Networking (BlackSeaCom)*, May 2014, pp. 83–87.

[10] B. Fleury, M. Tschudin, R. Heddergott, D. Dahlhaus, and K. I. Pedersen, "Channel parameter estimation in mobile radio environments using the sage algorithm," *IEEE Journal on Selected Areas in Communications*, vol. 17, no. 3, pp. 434–450, Mar 1999.

[11] A. Saleh and R. Valenzuela, "A statistical model for indoor multipath propagation," *IEEE Journal on Selected Areas in Communications*, vol. 5, no. 2, pp. 128–137, February 1987.

[12] A. Maltsev *et al.*, "IEEE P802.11 Wireless LANs Channel Models for 60 GHz WLAN Systems," IEEE, Tech. Rep., May 2010.

[13] J. Hartigan and M. Wong, "Algorithm AS 136: A k-means clustering algorithm," *Applied statistics*, pp. 100–108, 1979.